Applied Catalysis B: Environmental 84 (2008) 379–388

Contents lists available at ScienceDirect

Applied Catalysis B: Environmental

journal homepage: www.elsevier.com/locate/apcatb

Multivariate experimental design for the photocatalytic degradation of imipramine
Determination of the reaction pathway and identification of intermediate products

P. Calza [a], V.A. Sakkas [b,*], A. Villioti [b], C. Massolino [a], V. Boti [b], E. Pelizzetti [a], T. Albanis [b]

[a] Department of Analytical Chemistry, University of Torino, via P. Giuria 5, 10125 Torino, Italy
[b] Department of Chemistry, University of Ioannina, Panepistimioupoli, Ioannina 45110, Greece

ARTICLE INFO

Article history:
Received 26 February 2008
Received in revised form 5 April 2008
Accepted 12 April 2008
Available online 20 April 2008

Keywords:
Photo-Fenton
TiO_2
Mineralization
Toxicity
Central composite design

ABSTRACT

Multivariate experimental design was applied to the degradation of imipramine solutions under simulated solar irradiation. The efficiency of photocatalytic degradation was determined from the analysis of the following parameters: H_2O_2, $Fe^{(II)}$ and TiO_2 concentrations. Experimental data were then fitted using artificial neural networks (ANNs). The findings indicate that ANN provided excellent predictive performance while the influence of each parameter on the variable studied was assessed, TiO_2 being the most significant factor, followed by H_2O_2 and $Fe^{(II)}$.

TOC profile shows an initial sharp decrease within 4 h of irradiation (almost 75% of the organic carbon was mineralized) and until 24h complete mineralization is achieved. Nitrogen is mainly transformed into ammonium ions (almost 90% of the stoichiometric amount) and in a negligible extent into nitrate ions.

GC/MS and LC/MS were brought to bear in assessing the temporal course of the photocatalyzed process. A first pathway involves the hydroxylation, that is confined to the dibenzodiazepine moiety or the methyl groups. Another route proceeds through the oxidation of the dibenz[azepine] moiety, with the formation of the ketoderivative. Afterwards, the detachment of the aminoalkylic chain occurs. A parallel transformation involves aminoalkylic chain, with the partial or total detachment of the propylic chain.

Microtox bioassay (*Vibrio fischeri*) was also employed in evaluating the ecotoxicity of solutions treated by photocatalysis. Results clearly demonstrate the efficiency of the photocatalytic process in the detoxification of the irradiated solution.

1. Introduction

The issue of pharmaceutical (PhACs) as well as personal care products (PPCPs) and their metabolites in the environment has raised increasing concern in recent years. The discharge of therapeutic agents in effluents from production facilities, hospitals, as well as private households, and/or improper disposal of unused drugs, all lead to contamination of environmental waters, and wastewater-treatment plants (WWTPs) are considered to be a major source [1].

Although the concentration of these residues in the aquatic environment is too low to pose a very acute risk, it is unknown whether other receptors in non-target organisms are sensitive to individual residues, or the combination of drugs that share a common mechanism of action exhibits synergistic effects [2].

Over the last decade a new generation of antidepressants and antipsycotics has been developed. Among them imipramine (IMI), amitriptyline (AMI), and their respective demethyled metabolites desipramine (DES) and nortriptyline (NOR) which are active principles of four psychiatric drugs widely used to relieve symptoms of depression [3].

Initially, imipramine (the first tricyclic antidepressant to be developed by Ciba-Geigy) was tried against psychotic disorders (e.g. schizophrenia), but proved insufficient. This active ingredient is in fact well known to induce and exacerbate psychosis. To this day, imipramine is often considered the "Gold Standard" antidepressant as its ability to lift even the most severe depressive episodes is unsurpassed.

Because surface water is the most affected, PhACs may first pose a problem to utilities that use surface water as a source for drinking

* Corresponding author. Tel.: +30 26510 98363; fax: +30 26510 98795.
E-mail address: vsakkas@cc.uoi.gr (V.A. Sakkas).

0926-3373/$ – see front matter © 2008 Elsevier B.V. All rights reserved.
doi:10.1016/j.apcatb.2008.04.015

water production. Therefore, a crucial need for more enhanced technologies that can reduce their presence in the environment has become evident.

There is a group of chemical-oxidative processes called advanced oxidation processes (AOP), characterized by the generation of hydroxyl radicals, one of the strongest known oxidant. Therefore, it is possible for the hydroxyl radical to oxidize and mineralize almost every organic molecule into CO_2 and inorganic ions. AOPs such as H_2O_2/UV processes, Fenton and photo-Fenton catalytic reactions [4–6] and TiO_2 mediated photo-catalysis [7–9] have been widely used to destroy organic pollutants including PhACs and PPCPs [10–13].

To the best of our knowledge this is the first time that an extensive study of the photocatalyzed transformation of the pharmaceutical agent imipramine is examined. The main objectives of this research were to assess the degradation of the pollutant in several different aspects. Firstly in order to optimize the reagent concentrations involved in the degradation of the target molecule (namely TiO_2 and Fenton's reagent) a multivariate experimental design was performed employing artificial neural networks (ANNs). ANNs have already proved to play an important role in modelling and prediction of AOPs [14–18]. The use of ANNs allows the estimation of degradation efficiency of imipramine as a function of process parameters within the experimental range studied. Also the individual effect of each variable involved can be determined.

Another aspect of this work was the identification of possible intermediate products as well as the determination of the total mineralization during the process. For this reason powerful analytical techniques such as gas and liquid chromatography coupled to mass spectrometry and ion chromatography were employed. Moreover, in order to evaluate the toxicity of the irradiated solutions a bacterial assay was carried out based on the bioluminescence reduction of the marine bacterium *Vibrio fischeri*, using a Microtox Analyzer.

2. Experimental

2.1. Material and reagents

Experiments were carried out using TiO_2 Degussa P25 as the photocatalyst. In order to avoid possible interference from ions adsorbed on the photocatalyst, the TiO_2 powder was irradiated and washed with distilled water until no signal due to chloride, sulphate or sodium ions could be detected by ion chromatography.

Imipramine was purchased from Aldrich and has been used as received. HPLC grade water was obtained from MilliQ System Academie (Waters, Millipore). Acetonitrile HPLC grade (BDH) was filtered through a 0.45 μm filter before use. Ammonium acetate reagent grade was purchased from Fluka Chemie (Sigma). $FeSO_4{\cdot}7H_2O$ and H_2O_2 (30%, w/v) used as reagents were obtained by Merck.

2.2. Irradiation procedures

Irradiation experiments of imipramine were carried out on stirred aqueous solutions contained in a cylindrical quartz glass reactor. Degradation were performed on 50 ml of aqueous imipramine solutions containing the different initial concentrations of H_2O_2, $Fe^{(II)}$ and TiO_2, according to the experimental design. Irradiation was carried out using a Suntest CPS+ apparatus from Heraeus (Hanau, Germany) equipped with a xenon arc lamp (1500 W) and glass filters restricting the transmission of wavelengths below 290 nm. An average irradiation intensity of 750 W/m^2 was maintained throughout the experiments and was measured by internal radiometer. The corresponding light dose for 10 min of irradiation was 450 kJ/m^2. Chamber and black panel temperature were regulated by pressurized air-cooling circuit and monitored using thermocouples supplied by the manufacturer. The temperature of samples did not exceeded 20 °C using tap water cooling circuit for the UV-reactor. To remove TiO_2 particles the solution samples were passed through 0.45 μm HA cellulose acetate membrane filters and were further analyzed by the appropriate analytical technique.

Experiments on intermediates have been performed in air-saturated conditions using a 1500 W xenon lamp (Solarbox, CO.FO.MEGRA, Milan, Italy) simulating AM1 solar light and equipped with a 340 nm cut-off filter. The irradiation was carried out on 5 ml of suspension containing 15 mg/l imipramine and 200 mg/l TiO_2.

2.3. Analytical procedures

2.3.1. Liquid chromatography

For the intermediates study, the chromatographic separations followed by a MS analyzer were run on a C_{18} column Lichrosphere, 250 mm × 4.0 mm. Injection volume was 20 μl and flow rate 1000 μl/min. Gradient mobile phase composition (ammonium acetate 5 mM pH 5/acetonitrile) was adopted: 80/20 to 20/80 in 10 min.

A Surveyor mass spectrometer (Thermo Finnigan) equipped with an atmospheric pressure interface and an ESI ion source was used. The LC column effluent was delivered into the ion source using nitrogen as sheath and auxiliary gas. The cone voltage was set at 50 V value. The heated capillary value was maintained at 300 °C. The acquisition method used was previously optimized in the tuning sections for the parent compound (capillary, magnetic lenses and collimating octapoles voltages) in order to achieve the maximum of sensitivity. The tuning parameters adopted for ESI source have been the following: capillary voltage 2.5 V, RF lens bios 0.3 V, ion energy 1 V mass spectra were collected in full scan positive mode in the range 60–700 m/z.

2.3.2. Gas chromatography

In the experiments where kinetic studies have been performed, during illumination of the aqueous solution, samples of 2.0 ml were withdrawn from the reactor at specific time intervals. The aqueous samples were filtered through 0.45 μm Millipore disks to remove TiO_2 particles and were extracted with dichloromethane, dried with a small amount of Na_2SO_4 and finally analyzed by GC/MS.

A GC/MS, QP 5000 Shimadzu instrument equipped with a DB 5 MS column (J&W Scientific) of 30 m length and 0.25 i.d., coated with 5% phenyl 95% methylpolysiloxane was used under the following chromatographic conditions: injector temperature 240 °C, oven temperature program 150 °C (held for 2 min) ramped at 20 °C/min to 250 °C (10 min) followed by another ramp of 20 °C/min to 270 °C (held for 3 min). Helium was used as carrier gas at a flow of 1 ml/min. The temperatures of the ion source and the interface were set at 240 and 290 °C, respectively. The scan time was 21 min and 3.0 μl injections were made. The analyses of the compound was performed in the selected ion monitoring (SIM) mode. The ions (m/z) that were selected were: 85, 195, 280 for confirmation and 234 for quantitative purposes.

Moreover to confirm the intermediates identity, the samples subjected to 15, 45 and 120 min of irradiation were extracted in CH_2Cl_2, concentrated to 100 μl and analysed by GC/MS. A GC/MS spectrometer (Agilent 6890, series II) equipped with a 5% phenylmethylpolysiloxane column (Agilent HP-5; 30 m × 0.25 mm) mm) was used.

Table 1
Central composite experimental design and results for imipramine degradation

H_2O_2–x_1	$Fe^{(II)}$–x_2	TiO_2–x_3	$Degradation_{(exp)}$ (%)	$Degradation_{(calc)}$ (%)
−1	−1	−1	53.0	53.1
+1	−1	−1	65.2	64.8
−1	+1	−1	57.3	57.0
+1	+1	−1	68.4	68.9
−1	−1	+1	80.4	82.4
+1	−1	+1	85.5	86.5
−1	+1	+1	82.2	82.4
+1	+1	+1	86.8	86.5
0	0	0	90.0	89.7
0	0	0	89.9	89.7
(−α)	0	0	85.0	84.5
(+α)	0	0	88.9	89.5
0	(−α)	0	89.0	88.7
0	(+α)	0	90.9	90.6
0	0	(−α)	47.0	47.3
0	0	(+α)	84.0	83.0

H_2O_2–x_1 (mg/l)	$Fe^{(II)}$–x_2 (mg/l)	TiO_2–x_3 (mg/l)	Levels
552	5.688	970	(+α, +1.68)
48	0.648	30	(−α, −1.68)
450	4.688	780	(+1)
150	1.688	220	(−1)
300	3.168	500	0

2.3.3. Ion chromatography

A Dionex instrument was employed equipped with a conductimeter detector. The determination of ammonium ions was performed by adopting a column CS12A and 25 mM metansulphonic acid as eluent, at a flow rate of 1 ml/min. In such conditions, the retention time is 4.7 min. The anions were analysed by using a AS9HC anionic column and a mixture of $NaHCO_3$ 12 mM and K_2CO_3 5 mM at a flow rate of 1 ml/min. In such experimental conditions the retention time of nitrate is 9.58 min.

2.3.4. Total organic carbon analyzer

Total organic carbon (TOC) was measured on filtered suspensions using a Shimadzu TOC-5000 analyzer (catalytic oxidation on Pt at 680 °C). Calibration was achieved by injecting standards of potassium phthalate.

2.3.5. Toxicity measurements

The toxicity of an imipramine solution and of aqueous samples collected at different irradiation times, was examined by Microtox Model 500 Toxicity Analyzer. Toxicity was evaluated by monitoring changes in the natural emission of the luminescent bacteria *V. fischeri* when challenged with toxic compounds. Freeze-dried bacteria, reconstitution solution, diluent (2% NaCl) and an adjustment solution (non-toxic 22% sodium chloride) were obtained from Azur. Briefly, samples were tested in medium containing 2% sodium chloride, in five dilutions and luminescence was recorded after 5 and 15 min of incubation at 15 °C. The inhibition of the luminescence, compared with a toxic-free control to give the percentage of inhibition, was calculated following the established protocol using the Microtox calculation program.

2.4. Experimental design

The central composite design (CCD) [19] was applied to analyze the simultaneous effect of H_2O_2, $Fe^{(II)}$ and TiO_2 in the photocatalytic degradation process as well as to evaluate the interactions between the studied variables. The central composite design realized considered low (−) and high (+) levels, as well as central points (0) for the H_2O_2, $Fe^{(II)}$ and TiO_2 concentration, respectively. The experimental conditions for all experiments and the results (response factor (Y) corresponding to imipramine degradation (%) after 15 min of irradiation) obtained are summarized in Table 1. Statistica 7.0 (StatSoft, Inc. Tulsa, USA) statistical package was used to generate the experimental matrix.

2.5. Neural network strategy

Artificial neural networks (ANNs) are biologically inspired computer programs designed to simulate the way in which the human brain processes information. They have the ability to approximate virtually any function in a stable and efficient way and, for this reason, they can be applied to quantify a non-linear relationship between causal factors and responses by means of iterative training of data obtained from a designed experiment.

Neural networks are formed by input data vectors, neurons and output functions. Each connection between input and output data and neurons is made by weight factors W_{ij}, which determine the effect of the input variable i on the neuron j. Input variables are looked as number fluxes which feed the network structure and reach the output pattern. ANN optimization process [20,21] is based on a training procedure to decrease the error between ANN response and experimental response for a given set of input variables.

The network examined in our study contained three inputs, representing H_2O_2 (x_1), $Fe^{(II)}$ (x_2) and TiO_2 (x_3) concentrations, respectively. The output pattern comprised one neuron representing the photocatalytic efficiency, namely imipramine degradation (%) after 15 min of irradiation.

3. Results and discussion

3.1. Imipramine stability and photolysis

Preliminary experiments were carried out, before the development of the experimental design, to evaluate the extent of hydrolysis and photolysis processes on the imipramine transformation. Results obtained by the adsorption in the dark, hydrolysis as well as direct photolysis for a time period of 90 min prove that the above abiotic processes were scarcely responsible for the observed fast transformations when the solution was irradiated in the presence of the photocatalytic reagents H_2O_2, $Fe^{(II)}$, TiO_2.

3.2. Kinetics of disappearance

Several experimental results indicated that the destruction rates of photocatalytic oxidation of various organic contaminants over illuminated TiO_2 fitted the Langmuir–Hinshelwood kinetics model:

$$-r = \frac{dC}{dt} = \frac{kKC}{1 + KC}$$

where r is the oxidation rate of the reactant, C the concentration of the reactant, t the illumination time, k the reaction rate constant and K is the adsorption coefficient of the reactant. Recent publications, Ollis [22] and Emeline et al. [23] have shown that a pseudo-steady state analysis may be applied. Our data are consistent with the Langmuir–Hinshelwood model (plotting Ln C_o/C versus time represents a straight line, the slope of which upon linear regression equals the apparent first-order rate constant k_{app} – 1st order kinetics). However, according to these two studies, adsorption/desorption equilibrium is not established under irradiation and in catalysis achievements, such an equilibrium is a major requirement for the validity of the L–H model.

In our case due to the development of the multivariate approach the optimization-efficiency of the photocatalytic procedure was evaluated as the degradation (%) after 15 min of light irradiation (Table 1, 4th column).

3.2.1. Neural network fitting

The ANNs architecture was searched for by the Statistica software (Release 7.0 E, Statsoft, Inc, Tulsa, USA). The learning period was completed when minimum error was reached. In other words, the error function, which measures the difference between calculated and predicted output values, was minimised. Multilayer perceptrons as well as radial basis function networks with one to six hidden layers, respectively, were tested. Back propagation and conjugate gradient descent as training algorithms were applied for the suitable network searching. Simultaneously, the values of error, used to determine how a neural network is performing during iterative training and execution, were calculated.

The actual output values were compared against the predicted ones. The verification cases included in the data set of the tested neural networks were used as a check for good predictability of the selected ones. Poor agreements between the predicted values and the verification points indicated over-learning, that is, over-fitting which occurs when the algorithm is run for too long (and the network is too complex for the problem or the available quantity of data).

The optimal network structure discovered using as output the degradation (%) of imipramine was a multilayer perceptron. The final architecture was composed of three neurons in the hidden layer (3:3:1), the conjugate gradient descent was used as the training algorithm and was found on the 95th epoch. The training error was 0.016699 and the verification error was 0.007486 with a performance of 0.053023 and 0.015969, respectively. These findings indicate that ANN had not over-learnt and provided good predictive performance as depicted in Fig. 1 (r = 0.99887). The fifth column in Table 1 presents the calculated values by way of the modeling procedure by ANNs.

A sensitivity analysis on the inputs to a neural network was performed by the statistical software. This indicates which input variables are considered most important by that particular neural network. Sensitivity analysis can give important insights into the usefulness of individual variables. It often identifies variables that can be safely ignored in subsequent analyses, and key variables that must always be retained. In other words sensitivity analysis on the input variables for the neural network can be used in order to deduce the effect of each parameter on the variable studied. In this study, it is observed that TiO_2 (79%) is the most significant factor affecting the degradation kinetics of the target compound. Hydrogen peroxide (16%) also affects the photocatalytic efficiency with $Fe^{(II)}$ (5%) displaying the lowest effect.

With the optimized structure, this ANN can be then used to construct a response surface throughout the experimental space allowing the exploration of the optimum region without further need for the function equation knowledge.

The response surfaces (Fig. 2), obtained from ANNs simulation show the imipramine percentage degradation after 15 min of irradiation as a function of the codified values of H_2O_2–$Fe^{(II)}$ and H_2O_2–TiO_2 concentrations, respectively, where the darker regions indicate higher percentages of the response. These response surfaces allowed to define the optimum concentration ranges of reagents and to evaluate the role of each variable in the degradation process.

The surface region with maximum degradation percentage of imipramine (Fig. 2a) involves the range of 0.0–0.5 of codified TiO_2 values, which corresponds to concentrations between 500 and 640 mg/l. In this TiO_2 range, all H_2O_2 concentrations studied (48–552 mg/l) resulted in high mineralization, suggesting a limited influence of H_2O_2 concentration on imipramine degradation when titania is presented.

It can be seen that when the concentration of hydrogen peroxide increases, the degradation rate smoothly increases. This positive effect maybe attributed to the inhibition of electron–hole recombination at the semiconductor surface by accepting a photogenerated electron from the conduction band and thus promoting the charge separation (Eq. (1)):

$$e^-_{CB} + H_2O_2 \rightarrow OH^- + {}^\bullet OH \quad (1)$$

As shown in Fig. 2a the degradation rate increases proportionally to TiO_2 concentration, as expected, confirming the positive influence of the increased number of TiO_2 active sites on the process kinetics. At higher catalyst loading a slight decrease of imipramine degradation (%) was observed, irrespectively of the initial H_2O_2 concentration. The availability of active sites increases with catalyst loading, but the light penetration, and hence, the photoactivated volume of the suspension shrinks. Similar observations have been also reported in other studies on various organic substances [24,25]. In addition the decrease on the degradation rate at higher catalyst loading may be due to deactivation of activated molecules by collision with ground state molecules [26].

Simulation analysis of the effect of the H_2O_2 and $Fe^{(II)}$ variables on the degradation (%) of imipramine is depicted in three

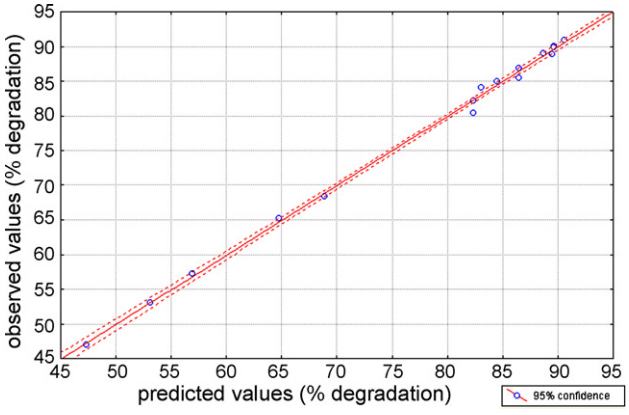

Fig. 1. Neural network fitting of the degradation (%) of imipramine under the photo-Fenton/TiO_2 system.

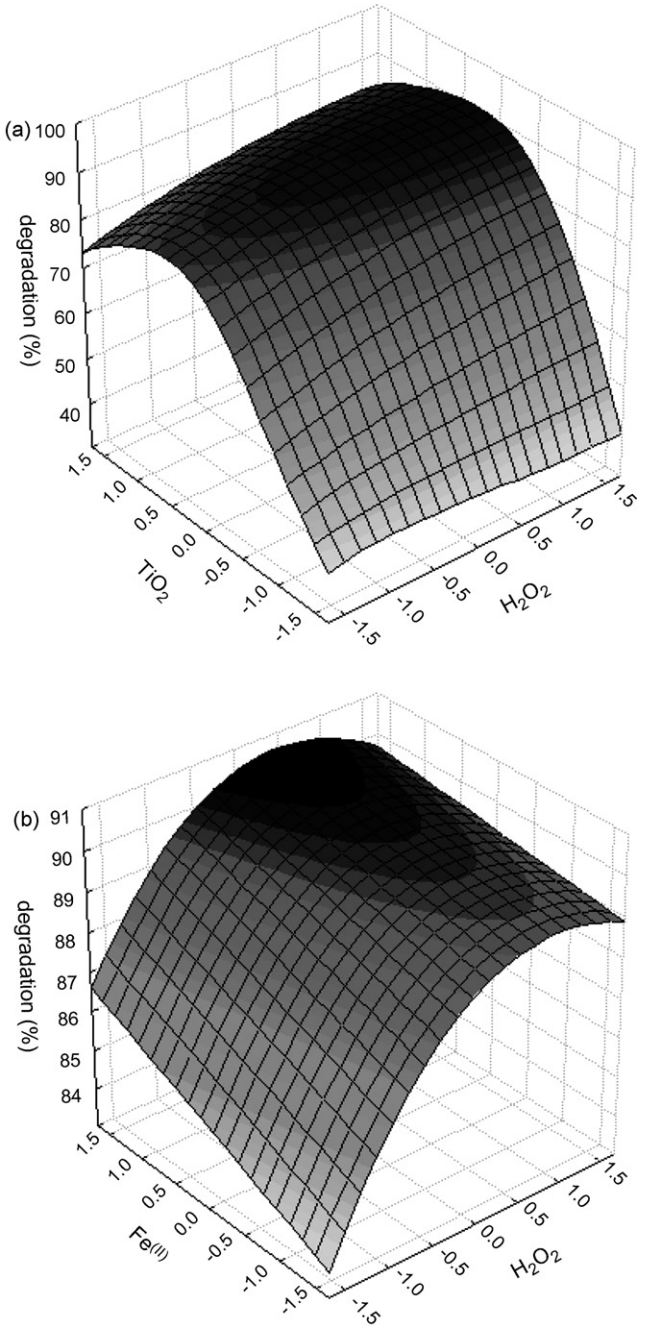

Fig. 2. ANNs simulation of the effect of (a) H_2O_2–TiO_2 concentration, (b) H_2O_2–$Fe^{(II)}$ concentration on the imipramine degradation (%) after 15 min irradiation.

dimensions in Fig. 2b. Results show that the photocatalytic efficiency increases as initial H_2O_2 concentration increases until reaching a maximum value. The higher reaction rates with increasing H_2O_2 can be attributed to the increase in the concentration of hydroxyl radicals. These radicals are generated by Eq. (1) while on the other hand, peroxide may be split photocatalytically to produce hydroxyl radical directly (Eq. (2)) or by reaction with superoxide anion (Eq. (3)) [15]:

$$H_2O_2 + h\nu \rightarrow 2^{\bullet}OH \quad (2)$$

$$H_2O_2 + O_2^- \rightarrow {}^{\bullet}OH + OH^- + O_2 \quad (3)$$

However when high concentrations of H_2O_2 are used, the degradation (%) diminishes since it may act as $^{\bullet}OH$ scavenger [27] reducing the amount of radicals available to destroy the imipramine molecules (Eq. (4)):

$$H_2O_2 + {}^{\bullet}OH \rightarrow HO_2^{\bullet} + H_2O \quad (4)$$

Although other radicals are produced ($HO_2^{\bullet}$) their oxidation potential is much smaller than the $^{\bullet}OH$ species [6].

The addition of $Fe^{(II)}$ slightly favors the degradation process and especially when low amounts of H_2O_2 are used. $Fe^{(II)}$ either reacts to form hydroxyl radicals (Eq. (5)) or to consume them (Eq. (6)) and the result of this competition is a small positive effect on the photocatalytic efficiency of imipramine.

$$Fe^{(II)} + H_2O_2 \rightarrow Fe^{(III)} + {}^{\bullet}OH + OH^- \quad (5)$$

$$Fe^{(II)} + {}^{\bullet}OH \rightarrow Fe^{(III)} + OH^- \quad (6)$$

Moreover, it has been reported that an excess of ferrous ions in the system (higher than those used in our study) may cause a decrease in the efficiency of degradation through the formation of ferryl ion intermediate (FeO_2^+) [5,28].

The optimal conditions for the highest photocatalytic efficiency (imipramine degradation: 90%) are H_2O_2 and TiO_2 concentration of 384 and 500 mg/l, respectively. For the photo-Fenton system the highest degradation percent obtained from the ANN simulation was 90.6% at concentrations of 363 and 5.688 mg/l for H_2O_2 and $Fe^{(II)}$, respectively. These optimal conditions have been experimentally confirmed demonstrating a degradation efficiency of 92 and 93%, respectively, after 15 min of illumination.

3.3. Imipramine transformation products

The study of the imipramine transformation products was performed in the presence of TiO_2 200 mg/l. Along with the drug decomposition, the formation of numerous intermediate compounds occurs. These organic compounds were detected by HPLC/MS and GC/MS and, on the basis of their *m/z* ratio and MS/MS main fragments, were attributed to the structures collected in Tables 2 and 3. The time evolution curves for the intermediates identified by HPLC/MS are shown in Fig. 3. A similar intermediate profile as a function of the irradiation time cannot be obtained for the compounds only detected by GC/MS, since only a selection of the irradiation samples have been analysed by GC (see Section 2.3.1).

Table 2 reports the intermediate products detected by HPLC/MS and/or GC/MS. Their identification was made by using an identification program by NIST library and also confirmed by HPLC/MS analysis through their MS/MS spectra analysis. For example, the protonated species at $[M+H]^+$ 297 affords methanol elimination, so indicating the location of an OH group on the methyl group; for instance, the species at $[M+H]^+$ 295 displays a CO loss, indicative of a keto group.

Table 3 shows the species only detected by HPLC/MS. All of them had retention times shorter than imipramine and, on the basis of their *m/z* ratio and MS/MS main fragments have been attributed to the structures depicted in Table 3. The imipramine MS/MS fragmentation study showed several peculiar losses, which will be carefully considered in identifying the unknown compounds formed during the imipramine photoinduced degradation:

(1) a base peak at *m/z* 86 (loss of dibenzo[b,f]azepine);
(2) a product ion at *m/z* 265 from the protonated molecule (*m/z* 281), due to the loss of a methane molecule;
(3) two product ions having *m/z* 236 (loss of dimethylamine) and 208 (loss of *N,N′*-dimethyl ethylamine).

Table 2
Imipramine and its intermediate compounds detected by HPLC/MS and GC/MS; molecular weight, retention times and structure

Name	M.W.	GC/MS (t_R)	HPLC/MS		Structure
			(t_R)	MS^2	
Imipramine (5*H*-dibenz[b,f]azepine-5-propanamine-10,11-dihydro-*N*,*N*′-dimethyl)	280	39.19	15.50	265 (50) ($-CH_4$); 236 (30) ($-C_2H_7N$); 208 (95) ($-C_4H_{11}N$); 86 (100) ($-C_{14}H_{13}N$)	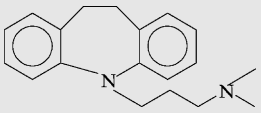
10*H*-Dibenz[b,f]azepine-10-one,5-(3-aminopropyl)5,11-dihydro	294	43.07	9.90	267 (30) (–CO)	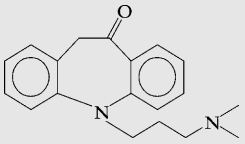
5*H*-Dibenz[b,f]azepine-5-propylamino-10, 11-dihydro-*N*-(methy) methanol	296	41.16	11.94	279 (30) ($-H_2O$); 265(25) ($-CH_3OH$)	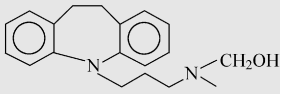
5-Ethanoldibenz[b,f]azepine	239	45.68 (15′		–	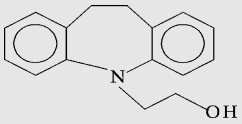
10,11-dihydro-5-methyl-5*H*-dibenz[b,f]azepine	209	32.37 (15′, 45′)	12.67	–	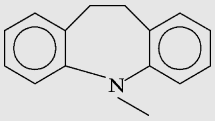
11-Hydroxy-5-*H*-dibenz[b,f]azepine	209	31.3 (15′)	12.00	182 (25) (–CO)	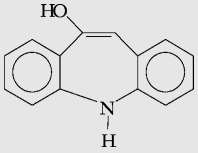
10,11-Dihydro-5*H*-dibenz[b,f]azepine	195	33.25 (15′)		–	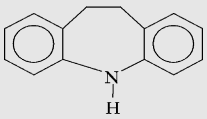
N(2-Propanyl dibenz[b,f]azepine	235	33.76 (15′)		–	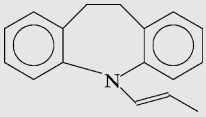
5*H*-Dibenz[b,f]azepine	193	22.25 (15′)		–	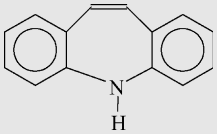
5-Methyldibenz[b,f]azapine-10-one	223	22.71	13.16	196 (20) (–CO)	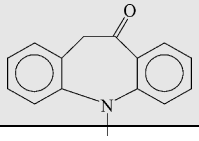

Several hydroxy and polihydroxy imipramine derivatives were formed and the exact position of the •OH radical attack can be tentatively deduced from their MS^2 fragmentation. The species at *m/z* 313, recognized as the bihydroxy imipramine derivative, displays a number of analogies between the produced fragments and those coming from imipramine MS/MS spectrum. Its major product ions derived by elimination of methane, dimethylamine and *N*,*N*′-dimethyl ethylamine; if combined with the presence of the product ion at *m/z* 86, it proves the presence of the amino alkylic chain unmodified. Thus, the two hydroxy groups are necessary located on the dibenzoazepine moiety, but the exact position for the substitution cannot be attributed.

Table 3
List of main $[M+H]^+$ and product ions coming from MS and MS^n spectra obtained from imipramine and its intermediate compounds only detected by HPLC/MS

$[M+H]^+$	t_R	MS/MS	Structure
313	9.92	297 (55) ($-CH_4$); 295 (10) ($-H_2O$); 279 (10) ($-H_2O$, CH_4); 268 (15) ($-C_2H_7N$); 240 (15) ($-C_4H_{11}N$); 86 (100) (−227)	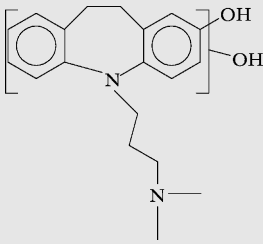
226	8.23	198 (60) (–CO); 180 (25) ($-H_2O$, –CO)	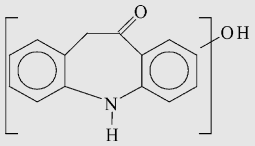
267	14.18	208 (30) ($-C_3H_9N$); 236 (20) ($-CH_5N$)	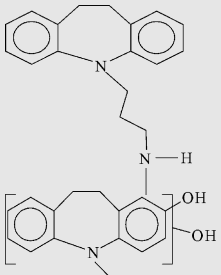
299	9.88	283 (100) ($-CH_4$)	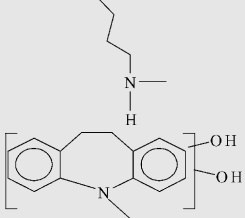
315	8.84	242 (80) ($-C_3H_7NO$) 279 (20) ($-2H_2O$); 268 (20) ($-NH_2CH_2OH$)	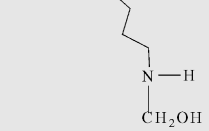

The species at *m/z* 267 eliminates methylamine (*m/z* 236) instead of dimethylamine, so proving the detachment of one of the two methyl groups. The species at *m/z* 299 can be attributed to the bihydroxylated derivative of the species at *m/z* 267, but the absence of peculiar losses does not permit to locate the two OH groups.

The formation of the species at *m/z* 315 is consistent with a trihydroxylation of the compound at *m/z* 267. The loss of amine methanol from the species at *m/z* 315 drove us to position an OH group on the methyl group, while the presence of the product ions at *m/z* 242 (loss of *N*-ethylamine methanol) excludes an OH attack to the propylic chain. Thus, the other two OH groups are necessary located on the dibenzoazepine moiety.

A structure at lower molecular weight, holding $[M+H]^+$ 226 was also identified. It originates two intense ions corresponding to the elimination of CO (*m/z* 198) and CO and water (*m/z* 180), that proves the presence of a keto group and of an hydroxyl group. The absence of the aminoalkylic peculiar losses suggests the detachment of the amino alkylic chain. Therefore, the keto and hydroxyl groups are necessary located in the benzodiazepine moiety.

3.4. Transformation pathways and mineralization

All the transformation products described above can be grouped as reported in Scheme 1. The initial transformation of imipramine proceeds through the occurrence of several concomitant pathways, labelled A–D. Hydroxylation involves the benzodiazepine moiety (pathway A) or one of the methyl groups (pathway B). Hydroxy and polydroxy derivatives are then easily transformed into the demethylated products. Alternatively, the transformation involves the aminoalkylic chain, with the detachment of the methyl amino group (pathway C). Subsequently, the progressive demethylation of the propylic chain occurs.

At the same time, another route proceeds through the oxidation of the dibenzoazepine moiety (pathway D), with the formation of the ketoderivative. Afterwards, the detachment of the aminoalkylic chain and the hydroxylation of the dibenzoazepine moiety occurs.

The intermediates described above were easily degraded, as assessed by Fig. 3, and after 2 h of irradiation they were completely degraded. At that time, almost 75% of the organic carbon and only

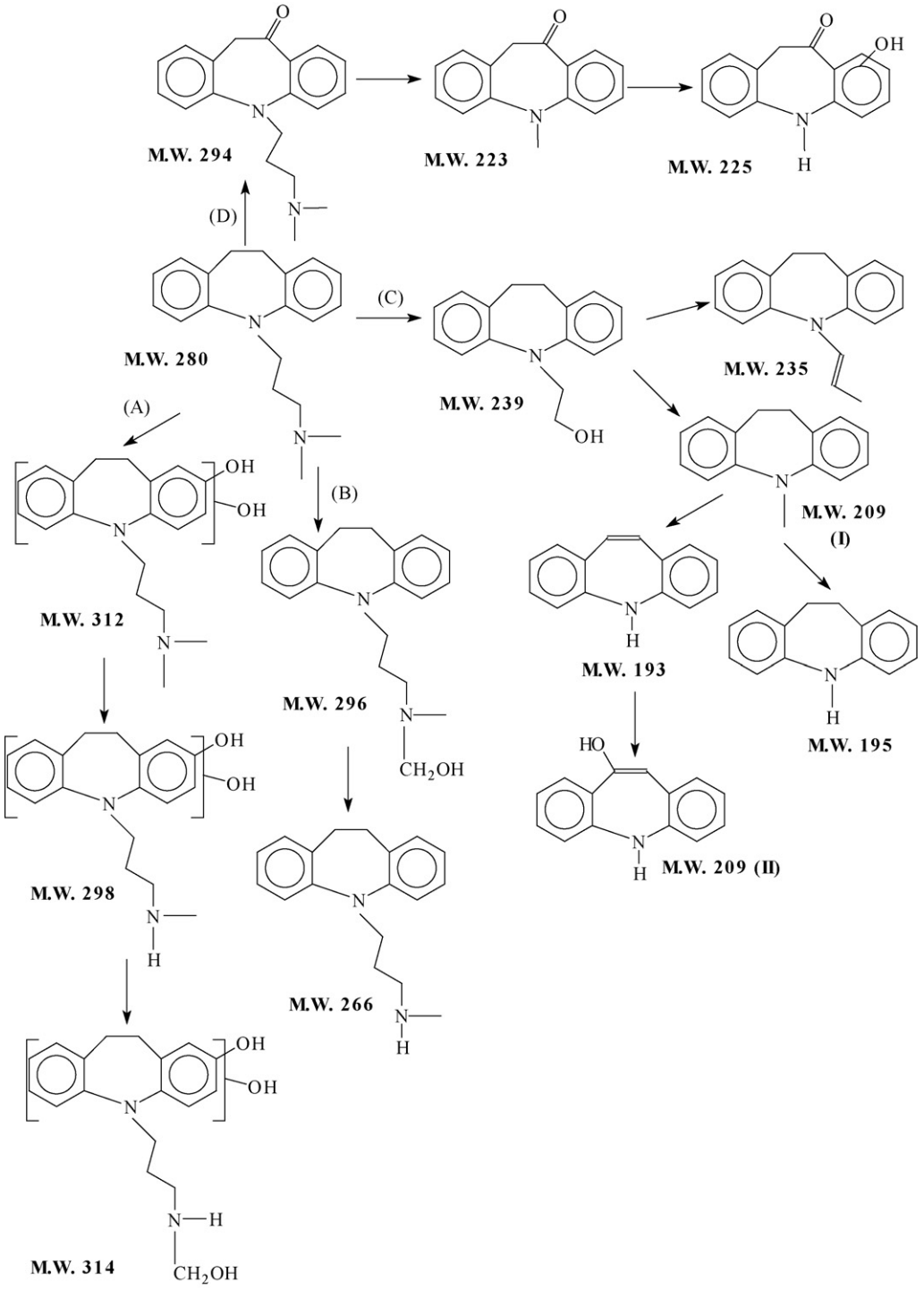

Scheme 1. Possible initial transformation pathways followed by imipramine under photocatalytic treatment.

30% of the organic nitrogen was mineralized (see Fig. 4). It proves that some derivatives still containing the organic nitrogen are formed. Even if imipramine completely disappears within 60 min of irradiation, the complete mineralization for organic carbon and nitrogen was only achieved after 24 h of irradiation. The nitrogen was mainly transformed into ammonium ions (almost 90% of the stoichiometric amount) and in a negligible extent into nitrate ions, as arise from Fig. 4. It is in agreement with the fate followed by alkylamines, that are known to be predominantly photoconverted to ammonium ions [29].

3.5. Toxicity evaluation

Several aqueous samples at different irradiation times were analyzed to estimate the percentage of inhibition of each sample. The initial toxicity of imipramine solution (0 h of

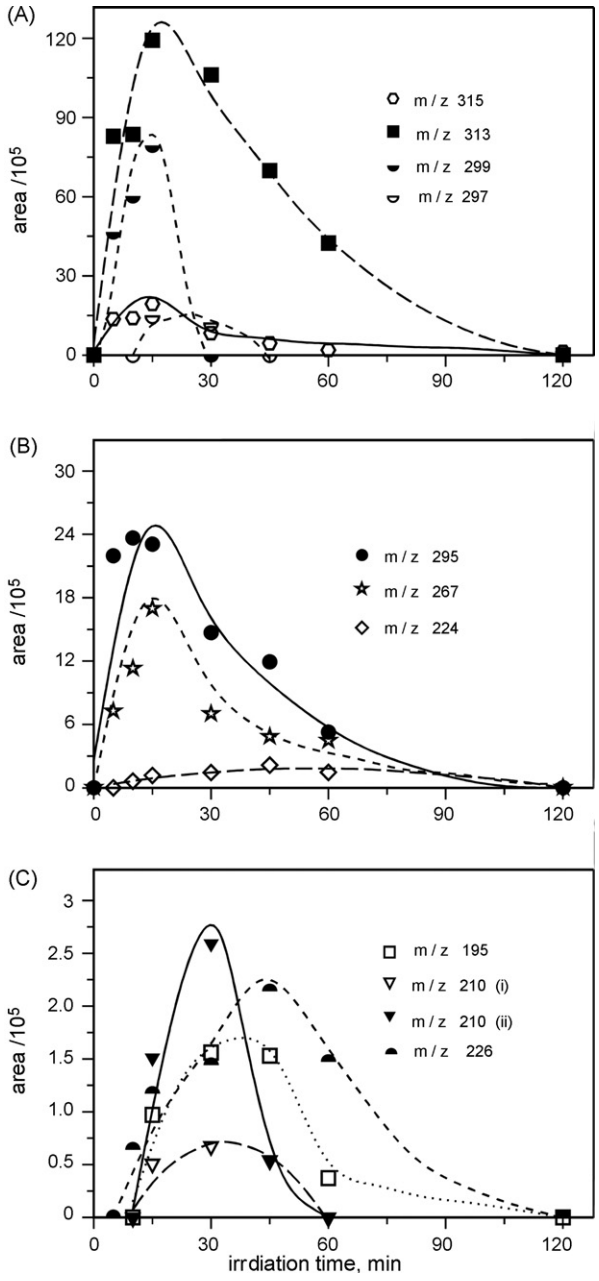

Fig. 3. (A–C) Intermediates formed from imipramine degradation as a function of the irradiation time.

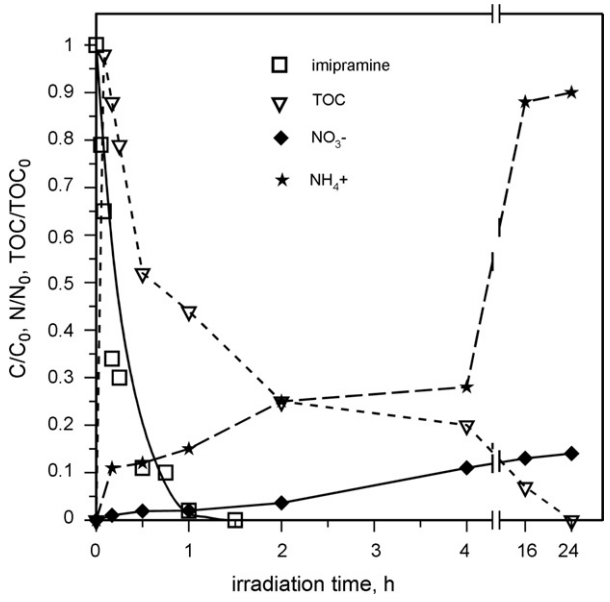

Fig. 4. Degradation of imipramine 15 mg l^{-1} on TiO_2 200 mg l^{-1}; disappearance of the initial compound, TOC profile and evolution of ammonium and nitrate ions.

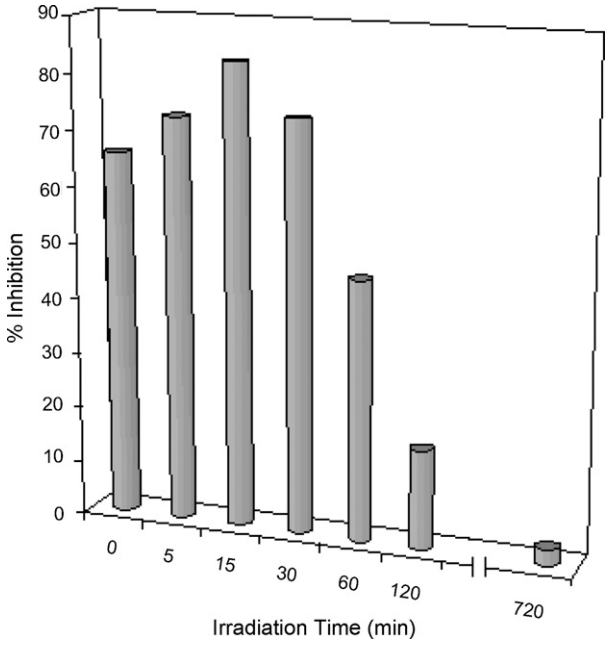

Fig. 5. Inhibition (%) of the luminescence of bacteria *Vibrio fischeri* as a function of the photocatalytic treatment time.

irradiation-distilled water) showed an inhibition of 66% that is slightly increased to 73% after just 5 min of irradiation. After that time, the toxicity of the solution still increases and reaches a maximum of 83% inhibition, at 15 min (Fig. 5). It is worth mentioning that the highest toxicity is observed at the irradiation times where all the identified transformation products are present. Even if a correlation between the intermediates formed and the toxicity can be seen, it has not been possible to assess which molecule is the responsible of the toxicity. After that time inhibition % decreases (30 min, inhibition 74%) but remains still higher compared to imipramine initial toxicity. These observations clearly demonstrate that transformation products more toxic than imipramine are formed, while synergistic effects among them are also considered. At higher irradiation times the toxicity is smoothly decreased (less than 3% at 720 min of irradiation) until complete detoxification of the irradiated solution is achieved.

4. Conclusions

The photo-induced transformation of imipramine was studied in aqueous solution using TiO_2 as a photocatalyst combined with H_2O_2 and $Fe^{(II)}$. The fate of the selected drug was followed through evaluation of different aspects: (1) kinetic study of the imipramine decomposition; (2) identification of degradation compounds formed by adopting a photocatalytic process; (3) assessment of total mineralization during the process; and (4) evaluation of the toxicity of the irradiated solutions. Experimental data were then

fitted using artificial neural networks (ANNs). The findings indicate that TiO_2 was the most significant factor affecting imipramine degradation, followed by H_2O_2 and $Fe^{(II)}$. Imipramine was transformed under photocatalytic treatment into numerous species. Dibenzodiazepine moiety was involved into hydroxylation or reduction reaction, while the substituents on the amino moiety are subjected to decarboxylation, followed by the cleavage of the propylic chain. As assessed by TOC measurements, complete mineralization was achieved within 24 h of irradiation. Contemporaneously, also the aminic group was completely transformed into inorganic ions, with the predominant formation of ammonium ions. Ecotoxicity measurements on the treated solutions emphasize the efficiency of the photocatalytic treatment in the detoxification process. Therefore, the photo-Fenton and TiO_2 system, demonstrates to be effective in wastewaters treatment/detoxification, while analytical characterization of unknown compounds by MS and toxicity monitoring revealed as fundamental tools to completely understand the degree of contamination or pollution of a water sample.

Acknowledgments

This research was financially supported by the project PENED (03ED926), of the Greek General Secretariat of Research and Technology. Financial support by Università di Torino-Ricerca Locale is also gratefully acknowledged.

References

[1] T. Kosjek, E. Heath, M. Petrovic, D. Barcelo, Trends Anal. Chem. 26 (11) (2007).
[2] M. Farre, I. Ferrer, A. Ginebreda, M. Figueras, L. Olivella, L. Tirapu, M. Vilanova, D. Barcelo, J. Chromatogr. A 938 (2001) 187.
[3] J.G. Hardman, L.E. Limbird, P.B. Molinoff, R.W.R. Ruddon, A.G. Gilman, in: J.G. Hardman, L.E. Limbird, A.G. Gilman (Eds.), Goodman and Gilman's The Pharmacological Basis of Therapeutics, McGraw-Hill, New York, NY, 1996.
[4] W.C. Paterlini, R.F. Pupo Nogueira, Chemosphere 58 (2005) 1107.
[5] M.J. Farre, X. Domenech, J. Pera, Water Res. 40 (2006) 2533.
[6] J.H. Ramirez, C.A. Costa, L.M. Madeira, Catal. Today 107/108 (2005) 68.
[7] I.K. Konstantinou, T.A. Albanis, Appl. Catal. B: Environ. 42 (2003) 319.
[8] A. Fujishima, K. Hashimoto, T. Watanabe, TiO_2 Photocatalysis, Fundamentals and Applications, Bkc Inc., Tokyo, 1999.
[9] J.M. Herrmann, J. Disdier, P. Pichat, S. Malato, J. Blanco, Appl. Catal. B: Environ. 17 (1998) 15.
[10] S. Esplugas, D.M. Bila, L.G.T. Krause, M. Dezotti, J. Hazard. Mater. 149 (2007) 631.
[11] C. Zwiener, F.H. Frimmel, Water Res. 34 (2000) 1881.
[12] V.A. Sakkas, P. Calza, C. Medana, A.E. Villioti, C. Baiocchi, E. Pelizzetti, T. Albanis, App. Catal. B: Environ. 77 (2007) 135.
[13] P. Calza, V.A. Sakkas, C. Medana, C. Baiocchi, A. Dimou, E. Pelizzetti, T. Albanis, Appl. Catal. B: Environ. 67 (2006) 197.
[14] A. Durán, J.M. Monteagudo, M. Mohedano, Appl. Catal. B: Environ. 65 (2006) 127.
[15] A. Durán, J.M. Monteagudo, Water Res. 41 (2007) 690.
[16] A. Durán, J.M. Monteagudo, I. San Martín, F. García-Peña, P. Coca, J. Hazard. Mater. 144 (2007) 132.
[17] A. Durán, J.M. Monteagudo, E. Amores, Chemosphere 71 (2008) 161.
[18] F.-L. Toma, S. Guessasma, D. Klein, G. Montavon, G. Bertrand, C. Coddet, J. Photochem. Photobiol. A: Chem. 165 (2004) 91.
[19] G.E.P. Box, W.G. Hunter, J.S. Hunter, Statistics for Experimenters: An Introduction to Design, Data Analysis and Model Building, Wiley, New York, 1978.
[20] J. Zupan, J. Gasteiger, Neural Networks for Chemists, VCH Publishers, New York/Germany, 1993.
[21] L. Jacob, E. Oliveros, O. Legrini, A.M. Braun, TiO_2-photocatalytic treatment of water. Reactor design and optimization experiments, in: D.F. Ollis, H. Al-Ekabi (Eds.), Photocatalytic Purification and Treatment of Water and Air, Elsevier Science Publishers, The Netherlands, 1993, p. 511.
[22] D.F. Ollis, J. Phys. Chem. B 109 (2005) 2439.
[23] A.V. Emeline, V.K. Ryabchuk, N. Serpone, J. Phys. Chem. B 109 (2005) 18515.
[24] C.M. So, M.Y. Cheng, J.C. Yu, P.K. Wong, Chemosphere 46 (2002) 905.
[25] K. Nohara, H. Hidaka, E. Pelizzetti, N. Serpone, J. Photochem. Photobiol. A: Chem. 102 (2/3) (1997) 265.
[26] K. Nohara, H. Hidaka, E. Pelizzetti, N. Serpone, Catal. Lett. 36 (1996) 115.
[27] J.M. Monteagudo, M. Carmona, A. Durán, Chemosphere 60 (2005) 1103.
[28] W.C. Bay, M.H. Groin, J. Am. Chem. Soc. 54 (1932) 2124.
[29] P. Calza, E. Pelizzetti, C. Minero, J. Appl. Electrochem. 35 (2005) 665.